Blueshift of the *A*-exciton peak in folded monolayer $1H$-MoS_2

Frank J. Crowne,[1,*,†] Matin Amani,[1,†] A. Glen Birdwell,[1,†] Matthew L. Chin,[1] Terrance P. O'Regan,[1] Sina Najmaei,[2] Zheng Liu,[3] Pulickel M. Ajayan,[2] Jun Lou,[2] and Madan Dubey[1]

[1]*Sensors and Electron Devices Directorate, U.S. Army Research Laboratory, Adelphi, Maryland 20783, USA*

[2]*Department of Mechanical Engineering and Materials Science, Rice University, Houston, Texas 77005, USA*

[3]*School of Materials Science and Engineering, School of Electrical and Electronic Engineering, Nanyang Technological, 639798 Singapore*

(Received 5 July 2013; revised manuscript received 20 September 2013; published 6 December 2013)

The large family of layered transition-metal dichalcogenides is widely believed to constitute a second family of two-dimensional (2D) semiconducting materials that can be used to create novel devices that complement those based on graphene. In many cases these materials have shown a transition from an indirect band gap in the bulk to a direct band gap in monolayer systems. In this work we experimentally show that folding a $1H$ molybdenum disulfide (MoS_2) layer results in a turbostratic stack with enhanced photoluminescence quantum yield and a significant shift to the blue by ∼90 meV. This is in contrast to the expected $2H$-MoS_2 band-structure characteristics, which include an indirect gap and quenched photoluminescence. We present a theoretical explanation for the origin of this behavior in terms of exciton screening.

DOI: 10.1103/PhysRevB.88.235302 PACS number(s): 78.55.Et, 73.21.−b, 79.60.Jv, 73.22.−f

I. INTRODUCTION

Transition-metal dichalcogenide compounds, in particular molybdenum disulfide (MoS_2), have become the focus of considerable interest in the past few years due to their great potential as a complementary material to graphene in advanced high-performance flexible/transparent digital electronics and optoelectronic circuits as well as for use in new quantum mechanical devices.[1,2] Bulk samples of MoS_2 are indirect-gap semiconductors, with an indirect band gap of 1.3 eV. This arises from the presence of two conduction band minima (CBMs) at different points in the Brillouin zone, one at the K point directly above the valence-band maximum (VBM) and the other of lower energy between the K and Γ points. The band gap is thus the energy difference between the lower-energy CBM and the VBM, making it indirect.

Bulk MoS_2 exists in two polytypes: hexagonally stacked $2H$-MoS_2 and tetragonal $1T$-MoS_2. All bulk samples discussed in this paper belong to the $2H$ polytype, which is constructed by stacking identical monolayers, each of which consists of six single-atom sublayers of pure sulfur and molybdenum whose stacking order is S-Mo-S-S-Mo-S. Each monolayer can be further subdivided into two noncentrosymmetric three-layer units, with the second unit rotated by 180° relative to the first and weakly coupled to the latter by van der Waals (vdW) interactions.[3] As the sample thickness is reduced down to a few atomic layers, the indirect band gap is observed to widen. Band-structure calculations suggest that this widening is due to a rapid increase in the energy of the lower CBM while the higher-energy CBM and the VBM move only slightly. For layer thicknesses down to a $2H$ monolayer, the lower CBM determines the band gap, and the band gap remains indirect. Because the S-S bonds in monolayer MoS_2 are weakly coupled, exfoliation allows this monolayer to be further divided, resulting in a three-atomic-layer sheet with a simple S-Mo-S stacking.[4,5] In this paper we adopt the nomenclature of Ataca *et al.*[3] and identify these layers as the $1H$-MoS_2 polytype, which, unlike the $2H$ polytype, no longer has a center of inversion. Remarkably, in $1H$-MoS_2 the two CBMs trade places in terms of energy, leaving the K-point CBM directly above the VBM, which is now increased by approximately 100 meV, and converting the band gap for a single $1H$ layer from indirect to direct. $1H$-MoS_2 is the first two-dimensional (2D) material artificially created by exfoliating a 3D indirect-gap material to exhibit an induced indirect-to-direct band-gap transition.[6] In addition to the change in band structure, lack of inversion symmetry also leads to second-harmonic generation[7] and a significant piezoelectric coefficient,[8] opening the door for $1H$-MoS_2 to be used in device applications based on valley-selective nonlinear-optical and spintronic interactions (e.g., controllable Raman and spin scattering effects).[9] Moreover, it has also motivated the development of photodetectors and light-emitting devices based on MoS_2.[10,11]

Like graphene, layers of $1H$-MoS_2 have very little resistance to bending and can be subjected to strains greater than ∼10% without failure.[12] Also like graphene,[13,14] these layers can be folded onto themselves to form coupled two-layer structures. Among the possible arrangements of folded two layers are some that mimic a $2H$-MoS_2 monolayer (Fig. 1). In this paper we discuss the photoluminescence (PL) and Raman spectra of folded $1H$-MoS_2 layers and characterize their electrical properties. We report that, in contrast to a true $2H$ stacked monolayer, a folded layer can exhibit PL emission which is blueshifted by approximately 90 meV, along with an enhanced photoluminescence quantum yield (QY) comparable to an unfolded $1H$ layer as reported by Splendiani and co-workers.[15] As progress is made towards forming complex heterostructures using 2D materials, it is important to understand the effects of rotational misalignment, poor interlayer coupling, or general turbostratic behavior on the band structure. This is especially true for dichalcogenide systems such as MoS_2, because the change from $2H$ to $1H$ results in a fundamental change in the material's electronic properties.

II. EXPERIMENTAL METHODS

Bulk MoS_2 films were grown directly by chemical vapor deposition (CVD) onto a 285 nm SiO_2/Si substrate using the

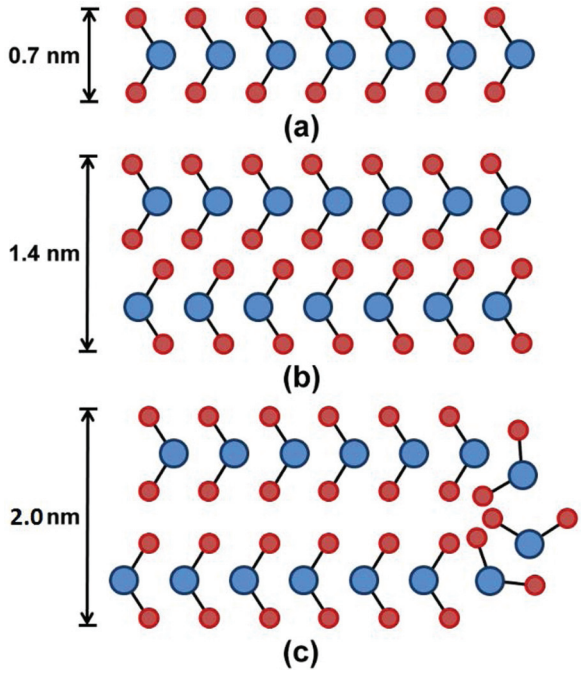

FIG. 1. (Color online) Schematics of a single $1H$-MoS_2 layer (a), single $2H$-MoS_2 monolayer (b), and folded $1H$-MoS_2 layer (c). Note the structural similarity of the latter to a $2H$-MoS_2 monolayer far from the connection region.

procedure described in detail by Najmaei and co-workers.[16] In brief, high-aspect-ratio MoO_3 nanoribbons were grown using hydrothermal processes, and then dispersed onto an auxiliary silicon substrate and placed inside a furnace tube with the growth substrate and sulfur powder. The furnace was heated to a peak temperature of 850 °C under a constant flow of nitrogen. Folded regions were created on these MoS_2 crystals by spinning a poly(methyl methacrylate) (PMMA) layer on the substrate and removing it in flowing acetone. This resulted in the stripping of a small fraction of the crystallites from the substrate and a smaller number being folded over onto themselves. Optical micrographs of these folded regions both before and after the folding occurred are shown in Fig. 2. Electron-beam lithography was then used to fabricate back-gated field-effect transistors (FETs) on these folded flakes of $1H$-MoS_2. The MoS_2 layers were patterned using a low-power inductively coupled plasma etch in a CH_4/O_2 plasma, and e-beam-evaporated Ti/Au (15/85 nm) was used to form source and drain contacts.

High-resolution Raman and photoluminescence imaging were performed after each processing step. These measurements were made using a WITec Alpha 300RA system using the 532 nm line of a frequency-doubled Nd:YAG laser as the excitation source. The spectra were measured in the backscattering configuration using a 100× objective and either a 600 or 1800 grooves/mm grating. The spot size of the laser was ∼342 nm, resulting in an incident laser power density of ∼140 $\mu W/\mu m^2$. Raman imaging found no time-dependent shifting of the E_{2g} or A_{1g} modes of $2H$-MoS_2 layers or the E' or A' modes[3] of $1H$-MoS_2 layers during testing. In addition, atomic force microscopy (AFM) and scanning electron microscopy (SEM) images were taken

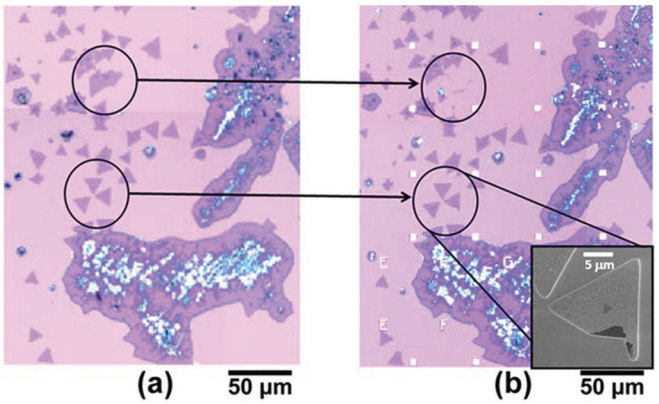

FIG. 2. (Color online) Examination of the circled regions in these before (a) and after (b) photographs reveals that processing can sometimes remove some triangles completely, while in other cases folds are generated in those triangles that have undergone partial detachment from the substrate. A backscatter SEM micrograph shown in the lower right of (b) reveals a large $1H$-MoS_2 folded region.

to verify layer count/height, and to search for residues left during processing. Field-effect mobilities of folded-layer and monolayer regions were measured with a Keithley 4200 semiconductor characterization system, using the substrate as a universal back gate. All electrical measurements were taken under high vacuum.

Figure 3 shows optical and scanning electron microscope images as well as atomic force microscope scans for a typical region around a fold. The step heights measured via AFM for our CVD-grown monolayer regions [Fig. 3(e)] are slightly thicker (∼1.0 nm) than what is normally observed for $1H$ layer material prepared by exfoliation (∼ 0.7 nm), whereas the measured $2H$ step height [Fig. 3(g)] is in very good agreement with the literature value. Despite the discrepancy between thickness measurements for exfoliated and CVD-grown $1H$-MoS_2 material, there is a strong consensus in the literature that CVD-grown samples like ours are in fact high-quality monolayers based upon independent evidence derived from annular dark-field scanning transmission electron microscopy, PL, and Raman spectroscopy.[17,18] We believe that the thickness discrepancy we measure is caused either by imperfect bonding between the SiO_2 and MoS_2 or by carbon contamination at the MoS_2-SiO_2 interface. The step height at the edge of the folded region is ∼2.0 nm, which is ∼0.6 nm larger than a $2H$-MoS_2 monolayer, as Figs. 3(d) and 3(f) show. The rms roughness measured for both the monolayer and folded-layer regions is 2.7 and 2.4 Å, respectively (measured SiO_2 roughness was 1.3 Å), which suggests that we have a defect-free MoS_2 to MoS_2 interface. In the Supplemental Material[19] we provide two sets of metrology results in addition to those shown in Fig. 3, which contain examples of folded regions. These results highlight the reproducibility of the blueshift and increased PL intensity for the folded $1H$-MoS_2 material relative to $2H$-MoS_2.

High-resolution Raman and PL intensity/position maps of the folded region are shown in Figs. 4 and 5, respectively. Figure 6 shows spectra averaged over an ∼1 μm^2 region for the $1H$ layer, $1H$ folded layer, and $2H$ monolayer regions. For the monolayer spectra we observed an average peak

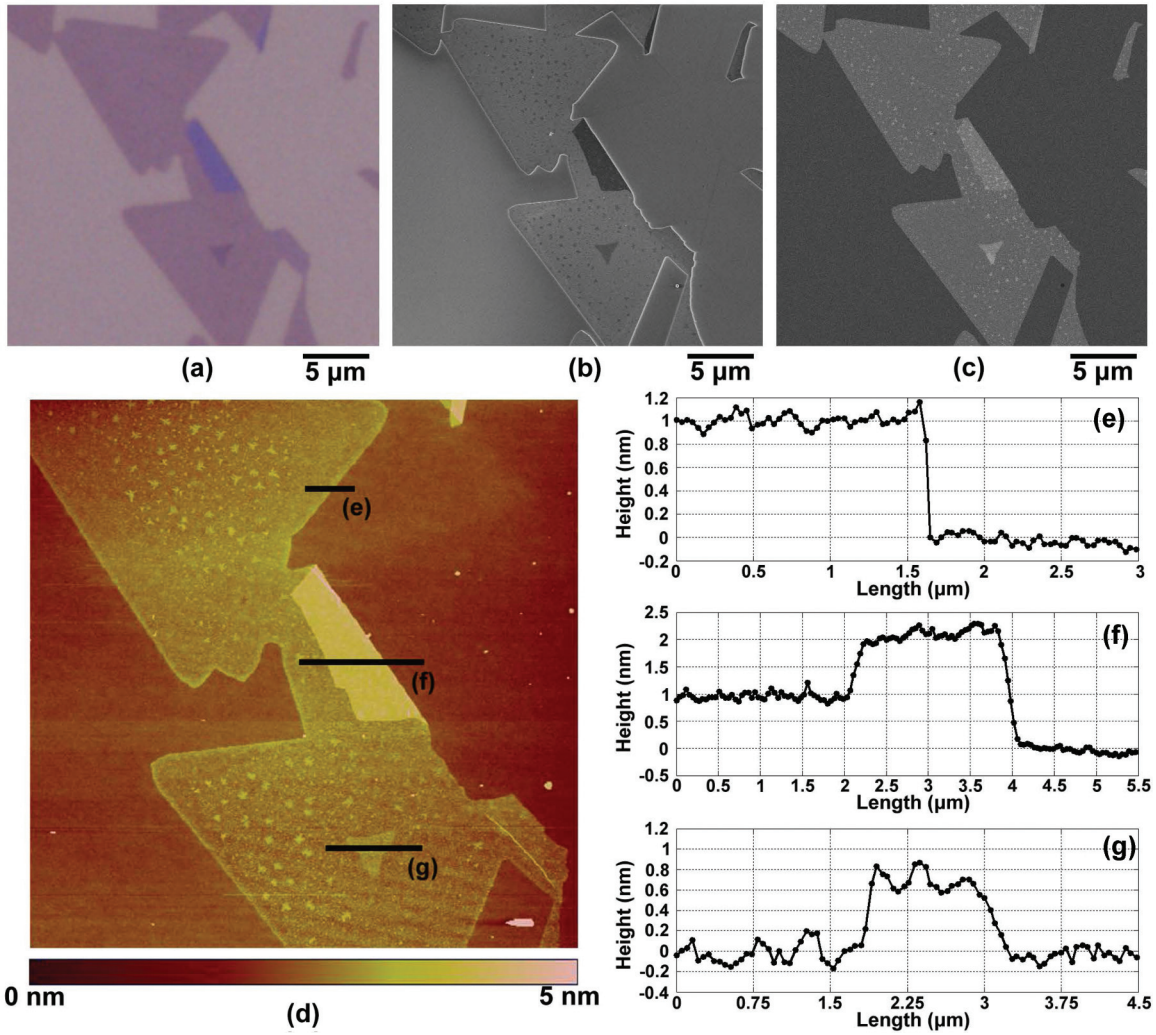

FIG. 3. (Color online) Optical (a), secondary electron (b), backscatter (c), and AFM (d) images of folded MoS_2, as well as corresponding scans from $1H$ layer (e), folded $1H$ layer (f), and $2H$ monolayer (g) regions.

separation of 21.6 cm^{-1} and an A'/E' intensity ratio of 1.8, in good agreement with descriptions of high-quality monolayer CVD-grown MoS_2 reported previously in the literature. For the case of the folded $1H$-MoS_2 layer we observe a hardening of the in-plane E' peak in the neighborhood of the fold, indicating the possible presence of increased doping and/or compressive strain.[12] The same trends are observed along the grain boundary defects in the MoS_2 crystal located directly above the fold. The corresponding PL mapping shows blueshifts of the A-exciton peak by as much as 90 meV in the folded region with no significant reduction in the QY compared to unfolded-layer material. In contrast, $2H$ stacked regions show the expected significant (in this case ~eightfold) reduction in the PL intensity of the A-exciton transition, indicating that the dominant transition is indirect.

We also fabricated a back-gated field-effect transistor on the folded MoS_2 region and compared the results with a device having the same geometry, but fabricated on a $1H$ layer within the same sample. Images of the device taken at various stages of the fabrication process are shown in Fig. 7 as well as I_{DS}-V_{BG} transfer curves for the two devices (both with a length $L = 800$ nm and width $W = 1$ μm) plotted on both logarithmic and linear scales. We see an expected increase in the saturation current for the folded sample; this is most likely due to the increase in sample thickness leading to a higher conductivity in saturation. Both the device built on the fold and the device built on a nearby pristine flake show very similar field-effect mobilities of 1.12 ± 0.15 and 0.95 ± 0.2 $cm^2/V\,s$, respectively, which are reasonable values for devices built on SiO_2 with no top dielectric (typical back-gated field-effect mobility values range from 0.5 to 8.0 $cm^2/V\,s$).[17] In the folded samples, the pinch-off voltage was significantly more negative, indicating that the folded region has a higher donor dopant density.

III. THEORY

The presence of a blueshift in the PL of this system is remarkably hard to explain, in that many potential causes, e.g., strain[20] or quantum confinement,[21] turn out to predict redshifts instead. After much discussion of our PL measurements, and the realization that the effect was manifested most strongly in the blueshift in the A-exciton peak, we focused our attention on excitons as possible enablers of the phenomenon. This was a

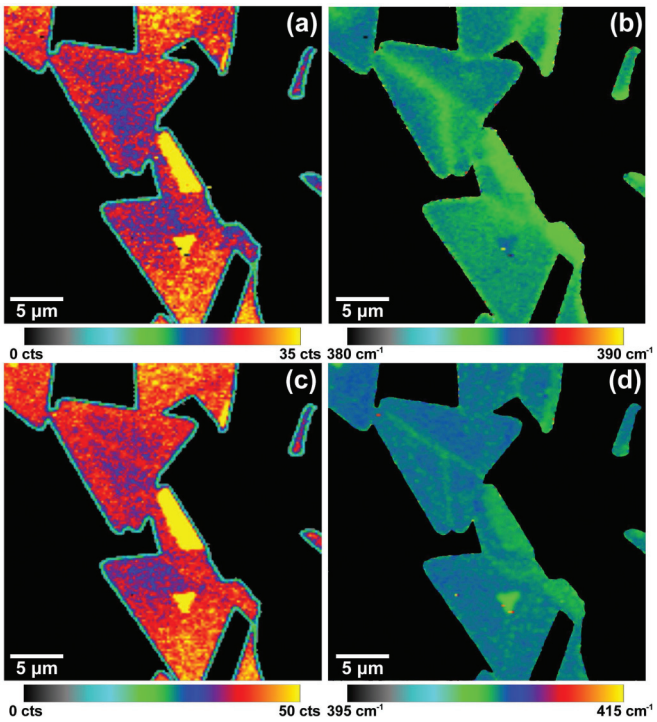

FIG. 4. (Color online) High-resolution maps of Raman peak intensity (a),(c) and position (b),(d) of the in-plane (a),(b) and out-of-plane (c),(d) modes in a folded $1H$-MoS_2 layer.

reasonable approach to take: in the course of PL measurements, the free carriers generated under illumination are usually assumed to equilibrate with a sizable population of excitons. Since both the conduction and valence bands of MoS_2 layers are built primarily out of d orbitals from the Mo atoms, with some small p-orbital admixture from the S atoms into the conduction band,[22,23] excitons in MoS_2 are highly localized, and are transitional between Frenkel type and Wannier type. The hybridized nature of the conduction band ensures that exciton recombination from the excitonic ground state is not inhibited by parity constraints. The translational motion of intact excitons is diffusive throughout the structure, and hence has no effect on, e.g., device electrical characteristics. In contrast, the free carriers created in PL do affect the device physics; in addition, they interact with the excitons via screening. This screening is anisotropic:[24] it is weak in

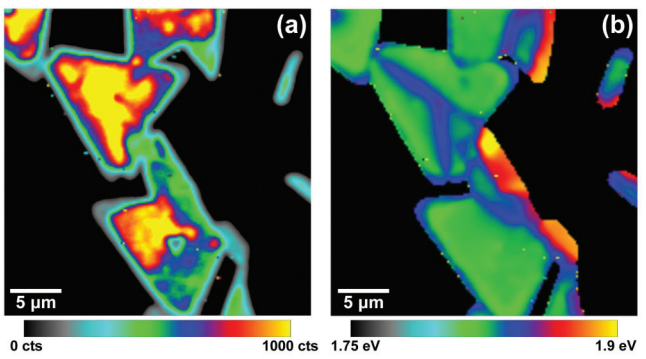

FIG. 5. (Color online) High-resolution maps showing the PL intensity (a) and peak position (b) in folded $1H$-MoS_2.

the direction perpendicular to the plane and strong parallel to the plane. This implies that the Coulomb forces between the exciton's electron and hole are stronger in the former direction and weaker in the latter directions. As a result, the excitons are "flattened" perpendicular to the Mo plane and spread out parallel to it.

A folded structure created from a single $1H$-MoS_2 layer brings a pair of monolayer "sheets" into close proximity. Figure 1 shows this process schematically. We note that in general the sheets will be misoriented; however, for folds along certain high-symmetry directions the folding results in a six-layer configuration with precisely the structure of a $2H$-MoS_2 monolayer, including the inversion of one sheet relative to the other. Because the band gap of this $2H$ monolayer is indirect and smaller than that of the 1H monolayer, we can infer that for this special orientation of the fold a *redshift* should appear in the PL when the sheets of the fold are *very* close. The question that then arises is whether a more remote separation or a turbostratic orientation of the sheets could lead to a blueshift. This line of inquiry led us to the model we describe below.

Figure 6(b) shows a comparison of the experimental PL curves for a $1H$-MoS_2 layer (blue), a folded $1H$-MoS_2 layer (red), and a $2H$-MoS_2 monolayer (green). Because the peaks shown are actually generated by exciton recombination light, we have based our explanation on the recombination kinetics of these excitons. As a result of the steady-state PL illumination, each sheet of the fold has its own population of excitons, which we label $\mathcal{X}_1$ and $\mathcal{X}_2$ for the top and bottom sheets, respectively. As the sheets approach one another, the excitons interact across the physical gap. At "large" distances the space between the sheets is empty, i.e., no free charge is present and all the charge is localized near the sheet atoms. This means that the fields in these regions are governed by Laplace's equation as in crystal-field theory and the theory of van der Waals forces, and hence can be expanded in multipole series whose structure is determined by the space-group symmetries of the atomic configurations. For an unperturbed 2D layer the charge density $\rho(\vec{X},z)$ will be periodic, allowing us to expand it in a 2D Fourier series:

$$\rho(\vec{X},z) = \frac{(2\pi)^2}{\Omega} \sum_{\vec{j}} \int_{\Omega} \rho(\vec{\Xi},z) e^{-i\vec{\Gamma}_{\vec{j}}\cdot(\vec{X}-\vec{\Xi})} d\vec{\Xi}.$$

Here $\vec{\Gamma}_{\vec{j}}$ are 2D reciprocal lattice vectors (RLVs) and Ω is the area of a unit cell of sheet material; note that the integral over $\vec{\Xi}$ is confined to a single unit cell. To obtain the corresponding (3D) electrostatic potential we use the Poisson equation:

$$\nabla^2\Phi(\vec{X},z) = \left(\frac{\partial^2}{\partial\vec{X}^2} + \frac{\partial^2}{\partial z^2}\right)\Phi(\vec{X},z) = \frac{1}{\varepsilon}\rho(\vec{X},z).$$

Although the density is zero outside the sheets, the potential is nonzero. Expanding this potential in the same way as the charge density,

$$\Phi(\vec{X},z) = \sum_{\vec{j}} e^{-i\vec{\Gamma}_{\vec{j}}\cdot\vec{X}} F_{\vec{j}}(z),$$

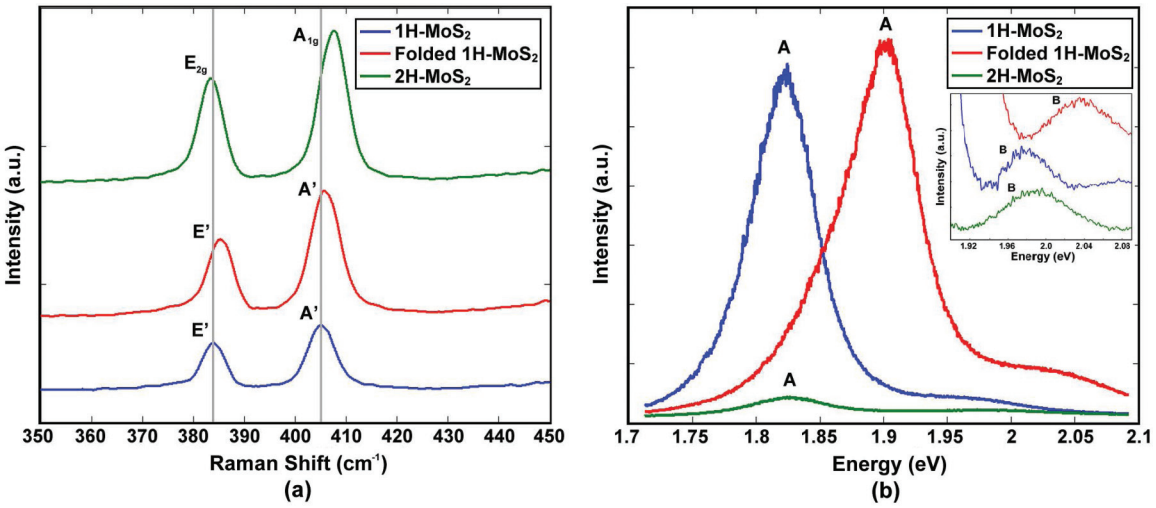

FIG. 6. (Color online) Raman (a) and PL (b) spectra for a $1H$-MoS_2 monolayer (blue), folded $1H$-MoS_2 (red), and a $2H$-MoS_2 monolayer (green). Inset: Expanded view of curves revealing the peak position of the B exciton.

allows us to find the z-dependent Fourier coefficients $F_{\vec{j}}(z)$ of the potential:

$$F_{\vec{j}}(z) = \frac{1}{2\Gamma_{\vec{j}}}\frac{1}{\varepsilon}\frac{1}{\Omega}\int_{\Omega} e^{i\vec{\Gamma}_{\vec{j}}\cdot\vec{\Xi}} d\vec{\Xi}\int_{-\infty}^{\infty} d\zeta e^{-|\vec{\Gamma}_{\vec{j}}||z-\zeta|}\rho(\vec{\Xi},\zeta).$$

If the region between the sheets is wide enough, only the longest-range fields are needed to describe the field from one sheet at the position of the other, i.e., those fields associated with the smallest $\vec{\Gamma}_{\vec{j}}$:

$$\Phi(z) \approx C_0 e^{-|\vec{\Gamma}_0|z}$$

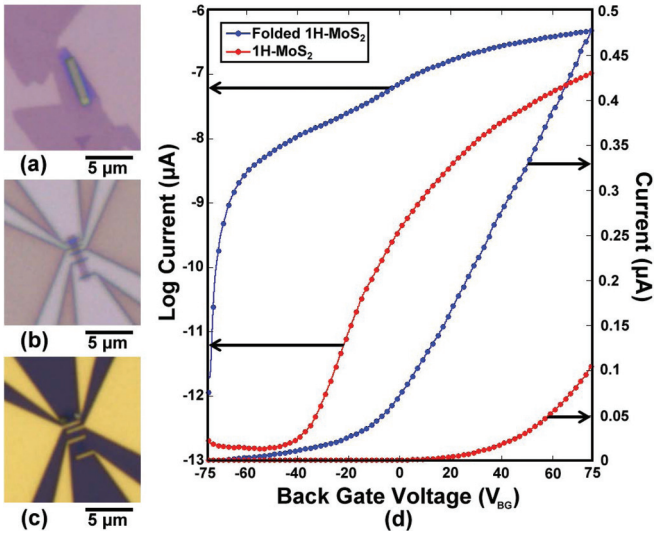

FIG. 7. (Color online) Optical micrographs depicting the fabrication flow of a back-gated FET on folded $1H$-MoS_2 (a)–(c): application of photoresist over the folded region (a), PMMA patterned to deposit Ohmic contacts on the etched region (b), and the finished device (c). I_{DS}-V_{BG} characteristics for both $1H$-MoS_2 (red) and folded $1H$-MoS_2 (blue) are plotted in both logarithmic and linear scales for an $L = 800$ nm, $W = 1$ μm FET measured using the two- point-probe technique (d).

where $\vec{\Gamma}_0$ is the smallest nonzero reciprocal lattice vector and

$$C_0 = \frac{1}{2|\vec{\Gamma}_0|}\frac{1}{\varepsilon}\frac{1}{\Omega}\int_{\Omega} d\vec{\Xi} e^{i\vec{\Gamma}_0\cdot\vec{\Xi}}\int_{-\infty}^{\infty} d\zeta e^{-|\vec{\Gamma}_0|\zeta}\rho(\vec{\Xi},\zeta)$$

is the field strength. For high-symmetry arrangements of the atoms within the sheets the integrals over $\vec{\Xi}$ will vanish and with them the fields of the smaller RLVs; thus, two high-symmetry sheets will interact only via the short-range vdW fields arising from the higher-order RLVs. This is especially significant for MoS_2, since the structure of a $2H$-MoS_2 (six-layer) monolayer possesses a center of inversion while the $1H$-MoS_2 (three-layer) structure does not. To see why, let us imagine folding a $1H$-MoS_2 layer along a line perpendicular to the picture shown in Fig. 1(a), i.e., so that it converts the two $1H$-MoS_2 sheets into a single $2H$-MoS_2 monolayer. Because this orientation will develop a center of inversion as the sheets approach each other, the long-range vdW fields between the $1H$-MoS_2 sheets will be suppressed and the excitonic energies for the two $1H$-MoS_2 sheets will be redshifted. If, however, the fold is along a low-symmetry direction, the two $1H$-MoS_2 sheets will be misoriented (turbostratic), and no center of inversion will develop, which will preserve the long-range vdW forces.

The existence of anomalously long-range electrostatic forces between turbostratic $1H$-MoS_2 sheets in close proximity has important implications for the kinetic theory of excitonic populations in a folded structure. Because excitons couple coherently to photons to form polaritons, recombination by photon emission is strongly inhibited;[25] however, this is not true for recombination via exciton-exciton collisions, which are by nature incoherent. Let us consider collisions that involve the annihilation of one of the excitons, i.e., reactions of the form

$$\mathcal{X} + \mathcal{X} \rightarrow \mathcal{X}^* + \Phi, \qquad (1)$$

where $\mathcal{X}^*$ is a final-state exciton in a ground or excited state and Φ denotes emission of either photons or phonons. Such a collision releases an energy $\mathcal{E}_G - \mathcal{E}_{\mathcal{X}}$, where $\mathcal{E}_G$ is the band gap and $\mathcal{E}_{\mathcal{X}}$ is the exciton binding energy; this

energy is available to excite the remaining exciton (requiring an energy $\mathcal{E}^*_{\mathcal{X}} - \mathcal{E}_{\mathcal{X}}$) and to generate the other particles (requiring an energy $\mathcal{E}_\Phi$). Conservation of energy implies that reactions of this kind will be exothermic as long as $\mathcal{E}_G - \mathcal{E}_{\mathcal{X}} > \mathcal{E}^*_{\mathcal{X}} - \mathcal{E}_{\mathcal{X}} + E_\Phi$. For Wannier excitons this inequality is easily satisfied since $\mathcal{E}_{\mathcal{X}}$ and $\mathcal{E}^*_{\mathcal{X}}$ are small (e.g., 4.8 and 3.0 meV in GaAs as measured from the conduction band), but for MoS_2 it is less obvious since some theoretical estimates predict values of $\mathcal{E}_{\mathcal{X}}$ in excess of 1 eV,[26,27] versus a value of 1.9 eV for $\mathcal{E}_G$.

More interesting is the reaction

$$\mathcal{X} + \mathcal{X} \rightarrow e^- + h^+ + \Phi \tag{2}$$

where e^- is a free electron, h^+ is a free hole, and Φ is a long-wavelength photon or multiple phonons, since energy conservation requires that $2\mathcal{E}_{\mathcal{X}} < \mathcal{E}_G$. Let us postulate that (2) can take place. If the two excitons are in the same sheet, the force that mediates this collision process should be in plane and dipolar in nature, and therefore inhibited by the strong in-plane screening. Suppose, however, that the excitons are in different sheets. Then the fields they carry may also extend into the gap like the vdW fields described above, making them available to mediate processes such as

$$\mathcal{X}_1 + \mathcal{X}_2 \rightarrow \begin{cases} e_1^- + h_2^+ + \Phi, \\ e_2^- + h_1^+ + \Phi. \end{cases} \tag{3}$$

The transition rate for these processes will involve a golden-rule process for breakup of both excitons plus the annihilation of one of the resulting electron-hole pairs:

$$R = \begin{cases} \sum_{\substack{\text{final} \\ \text{states}}} |\langle \mathcal{X}_1 \mathcal{X}_2 | H_{12} | e_1^- h_2^+ \Phi \rangle|^2 \delta \left(\mathcal{E}_{\mathcal{X}1} + \mathcal{E}_{\mathcal{X}2} - \varepsilon_{\mathrm{e}1} - \varepsilon_{\mathrm{h}2} - E_\Phi \right), \\ \sum_{\substack{\text{final} \\ \text{states}}} |\langle \mathcal{X}_1 \mathcal{X}_2 | H_{12} | h_1^+ e_2^- \Phi \rangle|^2 \delta \left(\mathcal{E}_{\mathcal{X}1} + \mathcal{E}_{\mathcal{X}2} - \varepsilon_{\mathrm{h}1} - \varepsilon_{\mathrm{e}2} - E_\Phi \right). \end{cases}$$

Here $H_{12} = H_{\mathrm{dip1}} + H_{\mathrm{dip2}} + H_{\mathrm{fold}} + H_R$ is the interaction between excitons in separate sheets, where $H_{\mathrm{dip1,2}}$ are exciton breakup operators, H_{fold} passes a free carrier from one sheet to another via the folded region, and H_R annihilates electron pairs, either radiatively or nonradiatively. The problem is reminiscent of Loudon's treatment of Raman scattering,[28] with the difference that the matrix element required is fourth order rather than third order as it is in the Raman case. Figure 8 shows one (of many) possible Feynman diagrams for process (3), in which both excitons break up virtually into electron-hole pairs within their respective sheets, followed by *nontunneling* transfer of a hole from one sheet to another in order to complete the annihilation of one of the excitons. The nontunneling path for this hole transfer is provided by the region where the sheets join together, i.e., the "bend" of the fold.

Because the screening in a 2D layer is anisotropic and weak in the direction perpendicular to the plane, Coulomb fields are enhanced in the intersheet gap relative to in-plane Coulomb fields. Because the intersheet gap is too wide for electrons and holes to tunnel across, the reaction products add to the screening free charge in both sheets. This in turn *reduces* the binding energy of the remaining excitons, leading to a blueshift in the recombination energy. If this blueshift is larger than the redshift of the free-carrier absorption edge, we will observe an overall blueshift in the PL.

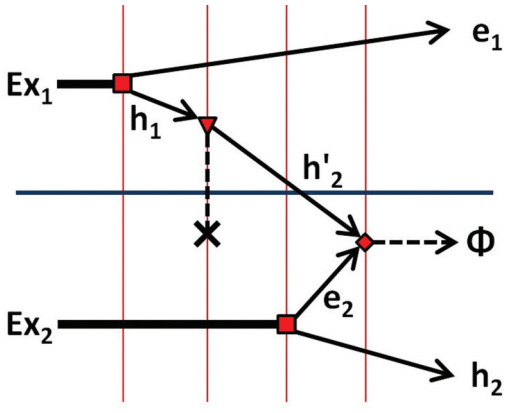

FIG. 8. (Color online) Feynman diagram for intersheet exciton-exciton collision. Exciton-*eh* vertices are denoted by squares, the diamond shows an *eh*-photon/phonon vertex, and the triangle shows intersheet *h*-*h* elastic scattering due to the fold edge. Red lines delineate the time ordering of this particular process. The symbol × denotes the vertex for converting hole h_1 into hole h'_2, i.e., transferring a hole from one sheet to another, via an infinitely heavy scatterer (see Ref. 29). The most likely agent for this process is nontunneling injection through the fold connection region.

IV. CONCLUSIONS

In summary, we report on our experimental studies of folded CVD-grown $1H$-MoS_2 monolayers. In marked contrast to the transition from an indirect- to a direct-band-gap material that occurs when a $2H$-MoS_2 monolayer is converted into a $1H$-MoS_2 layer, we observe that the reverse process of folding a $1H$-MoS_2 layer to form a nominally $2H$-MoS_2 monolayer does not lead to conversion back to an indirect-gap material and a redshift of the PL accompanied by a loss of QY. Rather, folding results in an anomalous enhanced photoluminescence coupled with a blueshift in the *A*-exciton peak by ~90 meV. We have proposed a theoretical explanation for our experimental observation that is able to explain the insensitivity to whether the sheets are in register or are rotated relative to one another. This is analogous to turbostratic stacking in graphene bilayers, and provides some insight into what types of behavior we can anticipate from turbostratic MoS_2 films. While the preservation of lack of inversion symmetry under folding could lead to new tunable electronic systems, such as valleytronic and nonlinear-optical devices and applications, 2D exciton phenomena in transition metal dichalcogenides will require further investigation before such advanced

device structures based on 2D interlayer interactions can be realized.

ACKNOWLEDGMENTS

The authors acknowledge the support of the US Army Research Laboratory (ARL) Director's Strategic Initiative (DSI) program on interfaces in stacked 2D atomic layered materials. The authors would also like to thank Pani Varanasi, ARO, for his in-depth technical discussion on 2D atomic layer R&D. P.M.A., J.L., S.N., and Z.L. also acknowledge funding support from the ARO MURI program on 2D materials. S.N. and Z.L. acknowledge funding support from Welch Foundation Grant C-1716 and the NSF Grant ECCS-1327093. Z.L. also acknowledges funding support in part by the Singapore National Research Foundation under NRF RF Award No. NRF-RF2013-08. The views and conclusions contained in this document are those of the authors and should not be interpreted as representing the official policies, either expressed or implied, of the ARL or the US Government. The US Government is authorized to reproduce or distribute reprints for Government purposes notwithstanding any copyright notation herein.

*Author to whom correspondence should be addressed: frank.j.crowne2.civ@mail.mil

†These authors equally contributed to this work.

[1] See, e.g., K. S. Novoselov *et al*., Proc. Natl. Acad. Sci. USA **102**, 10451 (2005).

[2] B. Radisavljevic, A. Radenovic, J. Brivio, V. Giacometti, and A. Kis, Nat. Nanotechnol. **6**, 147 (2011).

[3] C. Ataca, M. Topsakal, E. Aktürk, and S. Ciraci, J. Phys. Chem. C **115**, 16354 (2011).

[4] A. Ayari, E. Cobas, O. Ogundadegbe, and M. S. Fuhrer, J. Appl. Phys. **101**, 014507 (2007).

[5] S. Wu, J. S. Ross, G. B. Liu, G. Aivazian, A. Jones, Z. Fei, W. Zhu, D. Xiao, W. Yao, D. Cobden, and X. Xu, Nat. Phys. **9**, 149 (2013).

[6] K. F. Mak, C. Lee, J. Hone, J. Shan, and T. F. Heinz, Phys. Rev. Lett. **105**, 136805 (2010).

[7] N. Kumar, S. Najmaei, Q. Cui, F. Ceballos, P. M. Ajayan, J. Lou, and H. Zhao, Phys. Rev. B **87**, 161403(R) (2013).

[8] K. N. Duerloo, M. T. Ong, and E. J. Reed, J. Phys. Chem. Lett. **3**, 2871 (2012).

[9] D. Xiao, G. B. Liu, X. Feng, X. Xu, and W. Yao, Phys. Rev. Lett. **108**, 196802 (2012).

[10] H. S. Lee, S. W. Min, Y. G. Chang, M. K. Park, T. Nam, H. Kim, J. H. Kim, S. Ryu, and S. Im, Nano Lett. **12**, 3695 (2012).

[11] R. S. Sundaram, M. Engel, A. Lombardo, R. Krupke, A. C. Ferrari, Ph. Avouris, and M. Steiner, Nano Lett. **13**, 1416 (2013).

[12] P. Johari and V. B. Shenoy, ACS Nano **6**, 5449 (2012).

[13] Z. Ni, Y. Wang, T. Yu, Y. You, and Z. Shen, Phys. Rev. B **77**, 235403 (2008).

[14] P. Poncharal, A. Ayari, T. Michel, and J.-L. Sauvajol, Phys. Rev. B **79**, 195417 (2009).

[15] A. Splendiani, L. Sun, Y. Zhang, T. Li, J. Kim, C. Y. Chim, G. Galli, and F. Wang, Nano Lett. **10**, 1271 (2010).

[16] S. Najmaei, Z. Liu, W. Zhou, X. Zou, G. Si, S. Lei, B. I. Yakobson, J. C. Idrobo, P. M. Ajayan, and J. Lou, Nat. Mater. **12**, 754 (2013).

[17] W. Zhou, X. Zou, S. Najmaei, Z. Liu, Y. Shi, J. Kong, J. Lou, P. M. Ajayan, B. I. Yakobson, and J. C. Idrobo, Nano Lett. **13**, 2615 (2013).

[18] M. Amani, M. L. Chin, A. G. Birdwell, T. P. O'Regan, S. Najmaei, Z. Liu, P. M. Ajayan, J. Lou, and M. Dubey, Appl. Phys. Lett. **102**, 193107 (2013).

[19] See Supplemental Material at http://link.aps.org/supplemental/10.1103/PhysRevB.88.235302 for these two sets of metrology results.

[20] H.-L. Shi, Hui Pan, Y.-W. Zhang, and B. I. Yakobson, Phys. Rev. B **87**, 155304 (2013).

[21] D. A. B. Miller, D. S. Chemla, and S. Schmitt-Rink, Phys. Rev. B **33**, 6976 (1986).

[22] G. Eda, H. Yamaguchi, D. Voiry, T. Fujita, M. Chen, and M. Chhowalla, Nano Lett. **11**, 5111 (2011).

[23] K. F. Mak, K. He, C. Lee, G. H. Lee, J. Hone, T. F. Heinz, and J. Shan, Nat. Mater. **12**, 207 (2013).

[24] A. Fetter, Ann. Phys. (NY) **81**, 367 (1973); **88**, 1 (1974).

[25] C. Mavroyannis, Phys. Rev. B **1**, 2706 (1970).

[26] T. Cheiwchanchamnangij and W. R. L. Lambrecht, Phys. Rev. B **85**, 205302 (2012).

[27] A. Ramasubramaniam, Phys. Rev. B **86**, 115409 (2012).

[28] R. Loudon, Proc. R. Soc., London, Ser. A **275**, 218 (1963).

[29] S. Doniach and E. H. Sondheimer, *Green's Functions for Solid-State Physicists* (Addison-Wesley, Reading, MA, 1974), Sec. 5.2.